



## OPEN ACCESS

## EDITED BY

Yunyun Zhuang,  
Ocean University of China, China

## REVIEWED BY

Zhigang Zhou,  
Feed Research Institute (CAAS), China  
Jie Li,  
Yellow Sea Fisheries Research Institute  
(CAFS), China

## \*CORRESPONDENCE

Qingpi Yan  
yanqp@jmu.edu.cn

## SPECIALTY SECTION

This article was submitted to  
Microbial Symbioses,  
a section of the journal  
Frontiers in Marine Science

RECEIVED 06 July 2022

ACCEPTED 22 August 2022

PUBLISHED 13 September 2022

## CITATION

Wu W, Zhao L, Huang L, Qin Y,  
Zhang J, Zhang J and Yan Q (2022)  
Transcriptomic and metabolomic  
insights into the role of *fliS*  
in the pathogenicity of  
*Pseudomonas plecoglossicida*  
against *Epinephelus coioides*.  
*Front. Mar. Sci.* 9:987825.  
doi: 10.3389/fmars.2022.987825

## COPYRIGHT

© 2022 Wu, Zhao, Huang, Qin, Zhang,  
Zhang and Yan. This is an open-access  
article distributed under the terms of  
the [Creative Commons Attribution  
License \(CC BY\)](https://creativecommons.org/licenses/by/4.0/). The use, distribution  
or reproduction in other forums is  
permitted, provided the original  
author(s) and the copyright owner(s)  
are credited and that the original  
publication in this journal is cited, in  
accordance with accepted academic  
practice. No use, distribution or  
reproduction is permitted which does  
not comply with these terms.

# Transcriptomic and metabolomic insights into the role of *fliS* in the pathogenicity of *Pseudomonas plecoglossicida* against *Epinephelus coioides*

Wensi Wu<sup>1</sup>, Lingmin Zhao<sup>1</sup>, Lixing Huang<sup>1</sup>, Yingxue Qin<sup>1</sup>,  
Jiaonan Zhang<sup>2</sup>, Jiaolin Zhang<sup>2</sup> and Qingpi Yan<sup>1\*</sup>

<sup>1</sup>Fisheries College, Jimei University, Xiamen, China, <sup>2</sup>Key Laboratory of Special Aquatic Feed for Fujian, Fujian Tianma Technology Company Limited, Fuzhou, China

*Pseudomonas plecoglossicida* is responsible for visceral white spot disease in economically valuable marine fish such as *Larimichthys crocea* and *Epinephelus coioides*. Based on RNA sequencing, we previously showed that *P. plecoglossicida fliS* gene expression is significantly up-regulated in *E. coioides* spleens during infection. Here, to explore the role of this gene in pathogenicity, RNA interference (RNAi) was performed to silence *fliS* in *P. plecoglossicida*, and the mutant with the best silencing efficiency (89%) was chosen for further studies. Results showed that *fliS* silencing significantly attenuated motility, chemotaxis, adhesion, and biofilm formation of *P. plecoglossicida*. Furthermore, *E. coioides* infected with the *fliS*-RNAi strain recorded no deaths and showed fewer pathogens in the spleen and fewer white spots on the spleen surface compared to those fish infected with the wild type *P. plecoglossicida* strain. RNAi of *fliS* significantly affected the spleen transcriptome and metabolome in infected *E. coioides*. Kyoto Encyclopedia of Genes and Genomes (KEGG) analysis indicated that the cytokine-cytokine receptor interaction pathway was the most enriched immune-related pathway, and the arginine biosynthesis pathway was the most enriched metabolism-related pathway. These findings suggest that *fliS* is a virulence gene of *P. plecoglossicida* and is involved in the regulation of motility, chemotaxis, adhesion, and biofilm formation, as well as the inflammatory and immune responses of *E. coioides* to *P. plecoglossicida* infection.

## KEYWORDS

*Epinephelus coioides*, *Pseudomonas plecoglossicida*, *fliS*, pathogenicity, transcriptome, metabolome

## Introduction

The continuous emergence of various diseases remains a considerable challenge for the aquaculture industry (Borrego et al., 2017; Mugimba et al., 2021). *Pseudomonas plecoglossicida* is an opportunistic pathogen widely distributed in seawater and was originally isolated from cultured ayu (*Plecoglossus altivelis*) presenting with bacterial hemorrhagic ascites (Nishimori et al., 2000). More recently, it has been reported that *P. plecoglossicida* can infect *Larimichthys crocea* and *Epinephelus coioides* under low-temperature conditions, resulting in economically costly visceral white spot disease with high infection and mortality rates (Tang et al., 2020; Li et al., 2020). Pathogenicity is regulated by different genes, many of which are closely related to virulence regulation in aquatic pathogens, e.g., *toxR* in *Vibrio alginolyticus* (Cai et al., 2017), *sodA* and *sodB* in *Aeromonas hydrophila* (Zhang et al., 2019), and *exbB* and *fliG* in *P. plecoglossicida* (Jiao et al., 2021; Tang et al., 2022). However, despite extensive research on *P. plecoglossicida*, our understanding of its virulence genes remains poor. Previous dual RNA-seq data of *E. coioides* spleens infected with *P. plecoglossicida* (NCBI, SRP114910 and SRP115064) in our laboratory found that the *P. plecoglossicida* *fliS* gene was highly expressed in the host during infection (Luo et al., 2020), suggesting that this gene might be involved in the regulation of *P. plecoglossicida* virulence.

Bacterial flagella are complex motility organs composed of multiple protein subunits, including molecular motors, hook-basal-body complexes, and filaments (Lowenthal et al., 2009; Lertsethtakarn et al., 2011). Flagella are responsible for bacterial movement and are one of the factors that affect pathogenicity (Duan et al., 2013). The flagellum-specific export system is a specialized type III secretion system (T3SS) that exists in pathogenic bacteria for toxin export (Condry and Nilles, 2017; Miao et al., 2010), facilitated by special proteins called T3SS chaperones. The FliS protein, located in the flagellar hook, is a T3SS chaperone (Gu, 2017) that binds to the C-terminal region of flagellin to facilitate its export (Ozin et al., 2003; Muskotal et al., 2006). The *fliS* gene, which encodes FliS, is closely related to flagellum formation, motility, and bacterial toxicity (Yokoseki et al., 1995; Yokoseki et al., 1996). In *Yersinia pseudotuberculosis*, the *fliS* mutant strain has shorter flagella and weaker mobility. After complementation, the flagellum length of strain restored to wild type state (Xu et al., 2014). In addition, deletion of *fliS* in *Campylobacter jejuni* was reported to result in loss of motility and shorter flagella (Radomska et al., 2017). To date, however, the role of *fliS* in *P. plecoglossicida* pathogenicity has not yet been reported.

Given the considerable threat of *P. plecoglossicida* to cultured fish and the potential impact of *fliS* on bacterial virulence, we used RNA interference (RNAi) to silence the *fliS* gene in the *P. plecoglossicida* NZBD9 strain. We then explored differences in

virulence between the wild type and *fliS*-RNAi strains as well as differences in the immune response of *E. coioides* to different strain infection using transcriptomic and metabolomic sequencing and analysis.

## Materials and methods

### Bacterial strains and culture conditions

The pathogenic *P. plecoglossicida* strain (NZBD9) was isolated from the spleen of naturally infected *L. crocea* with white spot disease and stored at  $-80^{\circ}\text{C}$  (Luo et al., 2019). The *P. plecoglossicida* strain was routinely grown in Luria Bertani (LB) broth at 18 or  $28^{\circ}\text{C}$  with shaking at 220 rpm. *Escherichia coli* DH5 $\alpha$  was obtained from TransGen Biotech (Beijing, China) and grown in LB broth at  $37^{\circ}\text{C}$  with shaking at 220 rpm.

### Construction of *P. plecoglossicida* RNAi strain

The RNAi strain was constructed based on previous study (Luo et al., 2020). The sequences of five pairs of short hairpin RNA (shRNA) were designed according to the sequences of the *fliS* gene using RNAi Designer (<http://rnaidesigner.thermofisher.com>) and are provided in Supplementary Table 1. The five pairs of shRNAs were annealed and ligated to the linearized pCM130/tac vector. The recombinant pCM130/tac vector was transformed into competent *E. coli* DH5 $\alpha$  by heat shock, and competent *P. plecoglossicida* was eventually electrotransformed. The tetracycline resistance marker (10  $\mu\text{g}/\text{mL}$ ; final concentration) was used for screening stably silenced clones. The mRNA levels of *fliS* in the five mutants were determined by quantitative real-time polymerase chain reaction (qRT-PCR).

### Growth rate assay

Overnight culture of *P. plecoglossicida* in LB broth was adjusted to an optical density at 600 nm ( $\text{OD}_{600\text{ nm}}$ ) of 0.1 and diluted 10 000-fold with fresh LB broth. Aliquots (200  $\mu\text{L}$ ) of the diluted bacterial culture were added to 10 wells of a microtiter plate, then incubated at  $28^{\circ}\text{C}$ . The  $\text{OD}_{600\text{ nm}}$  of each well was automatically detected each hour for 48 h.

### Soft agar plate motility assay

Swarming motility was determined following previously described methods (Zuo et al., 2019). After overnight

cultivation in LB medium,  $OD_{600\text{ nm}}$  was adjusted to 0.2. The bacterial suspension (1  $\mu\text{L}$ ) was inoculated on semisolid agar plates. The plates were incubated at 28°C for 10–16 h to determine colony diameter. Three replicates were performed per group.

## Biofilm formation assay

Biofilm formation was explored following previous research (Jiao et al., 2021). *P. plecoglossicida* in the exponential growth period was adjusted to  $OD_{600\text{ nm}} = 0.2$  with fresh LB broth. Then, 100  $\mu\text{L}$  of diluted bacterial suspension was added into each well of a 96-well plate and incubated at 28°C for 24 h. Subsequently, each well was washed twice with 200  $\mu\text{L}$  of sterile phosphate-buffered saline (PBS), stained with 125  $\mu\text{L}$  of crystal violet (0.1%) for 15 min, washed three times with sterile PBS, and dried under sterile conditions. Finally, 200  $\mu\text{L}$  of 33% acetic acid was added to dissolve the dyed biofilm. The  $OD_{590\text{ nm}}$  of each well was measured, and each strain was repeated 10 times independently.

## Chemotaxis assay

Overnight culture of *P. plecoglossicida* was adjusted with sterile PBS to  $OD_{600\text{ nm}} = 1.0$ , and the bacterial suspension (0.25 mL) was then aspirated into a sterile syringe (1 mL). The open end of a capillary tube (inner diameter 0.1 mm, sealed at one end) was filled with *E. coioides* skin mucus (3  $\mu\text{L}$ ), horizontally dipped into the bacterial suspension in the syringe, then incubated at 28°C for 1 h. Finally, the number of bacteria in the mucus was determined by plate counting (Mao et al., 2020). Sterile PBS in a capillary tube was used as the control. Three independent biological replicates were performed per group.

## In vitro adhesion assay

*In vitro* adhesion was determined following previous study (He et al., 2021). First, sterile mucus of *E. coioides* (20  $\mu\text{L}$ ) was evenly coated onto a slide and fixed with 200  $\mu\text{L}$  of 4% methanol for 30 min. Then, 200  $\mu\text{L}$  of bacterial suspension ( $OD_{600\text{ nm}} = 0.3$ ) was evenly coated on the area with mucus. After the slides were incubated at 28°C for 2 h, they were washed three times with PBS to remove adherent cells. The bacterial cells adhered to the glass slide were fixed with 200  $\mu\text{L}$  of 4% methanol for 30 min and stained with 0.1% crystal violet for 3 min, after which the unstained crystal violet was washed with PBS. Five slides were performed per group, and the adhered bacteria in 20 randomly selected fields were counted under a microscope ( $\times 1\,000$ ) (Leica DM4000 B LED, Leica, Germany).

## Fish infection and sampling

Healthy size-matched *E. coioides* ( $14.7 \pm 0.7$  cm in length) were purchased from Zhangzhou city (Fujian, China) and adaptively maintained at 18°C for one week in laboratory seawater (water volume 320 L; pH = 7.8–8.2; continuous oxygen). The seawater temperature remained at  $18 \pm 1^\circ\text{C}$  throughout the experiment.

For survival rate assay, 60 fish were randomly divided into three groups: i.e., *fliS*-RNAi strain group, wild type strain group, and PBS group. Each fish in the infection groups was intraperitoneally injected with the corresponding strain at a dose of  $5 \times 10^4$  colony-forming units (CFU)/fish. For the negative control, 20 fish were injected with 200  $\mu\text{L}$  of PBS. Survival was observed and recorded every 12 h after injection to 10 days post infection (dpi).

For spleen sampling, 240 fish were randomly divided into three groups: i.e., wild type strain infection group, *fliS*-RNAi strain infection group, and PBS injection group. The fish were treated as described above. Six spleens were randomly sampled from each group at 1, 2, and 3 dpi. Two spleens from each group were randomly mixed into one sample and subjected to bacterial load and gene expression assays. Thirty-six spleens were randomly sampled at 4 dpi, with six spleens from the same group randomly mixed into one sample and subjected to qRT-PCR, pathogen load assay, *fliS* gene expression determination, and metabolomic analysis. All spleen samples were frozen in liquid nitrogen and stored in a refrigerator at  $-80^\circ\text{C}$ .

## qRT-PCR

qRT-PCR was performed using a QuantStudio 6 Flex Real-Time PCR system (Life Technologies, Carlsbad, CA, USA). Primers were synthesized by Tsingke Biotechnology Co., Ltd., (China) as shown in Supplementary Table 2. The *fliS* gene expression levels of *P. plecoglossicida* were normalized using 16S rDNA. Pathogen load of *P. plecoglossicida* in the infected spleens was determined based on the copy number of the housekeeping gene *gyrB* (Xin et al., 2020). Relative gene expression in the different groups was calculated using the  $2^{-\Delta\Delta\text{CT}}$  method (Luo et al., 2020).

## Transcriptomic analysis

An Illumina TruSeq™ RNA Sample Prep Kit was used for the RNA sequencing (RNA-seq) libraries. Total RNA was extracted from spleen samples, with RNA concentration and purity detected using a Nanodrop 2000 spectrophotometer. The RNA integrity number (RIN) was determined using an Agilent 2100 bioanalyzer. Oligo-dT was used to enrich mRNA, fragmentation buffer was

added to fragment mRNA, cDNA was reverse synthesized, and adapters were ligated. Sequencing was performed using the Illumina NovaSeq 6000 sequencing platform by Majorbio Biotechnology Co., Ltd. (Shanghai, China).

Raw Illumina reads were trimmed and quality-controlled (QC) using fastp to obtain high-quality clean data to ensure the accuracy of subsequent analyses. The clean reads of each sample were compared with the reference sequences assembled by Trinity to obtain the mapping results of each sample and for subsequent unigene and transcript quantification of each sample.

To explore the related biological processes, BLAST2GO was used for Gene Ontology (GO) annotation (Diao et al., 2019) and molecular annotation of differentially expressed transcripts of samples. Differentially expressed genes (DEGs) of transcripts between the *fliS*-RNAi strain infection (experimental) and the wild type strain infection groups (control) were analyzed using edgeR (screening criteria:  $|\log_2FC| \geq 1$  and false discovery rate (FDR) < 0.05). GO enrichment analysis was performed on the obtained transcripts using GOATOOLS. Signaling pathway functional enrichment was analyzed by Kyoto Encyclopedia of Genes and Genomes (KEGG) (Zhao et al., 2018). KOBAS (<http://kobas.cbi.pku.edu.cn/home.do>) were used for KEGG pathway analysis of differential transcripts. Ten genes were randomly selected to verify the reliability of RNA-seq by qRT-PCR.

## Metabolomic analysis

A certain amount of sample was accurately weighed and added to the extract obtained from the metabolite extraction process in a low-temperature environment. After centrifugation, the supernatant was collected for liquid chromatography-mass spectrometry (LC-MS) detection. Six replicates were performed per group.

LC-MS was performed using ultra-performance liquid chromatography tandem Fourier transform mass spectrometry (UPLC-MS/MS) with the UHPLC-Q Exactive HF-X system (Thermo Fisher). Chromatographic conditions were as follows: Acquity UPLC HSS T3 column (100 mm × 2.1 mm i.d., 1.8 μm); Waters, Milford, USA); mobile phase A 95% water + 5% acetonitrile (containing 0.1% formic acid) and mobile phase B 47.5% acetonitrile + 47.5% isopropanol + 5% water (containing 0.1% formic acid); injection volume 2 μL; column temperature 40°C. For mass spectrometry, the sample was subjected to electrospray ionization and mass spectrometry signals were collected in positive and negative ion scanning modes. Specific parameters are provided in [Supplementary Table 3](#).

After UPLC-TOF/MS, the raw data were preprocessed, including original data missing value filtering, missing value

filling, data normalization, QC verification, and data conversion. In addition, mass spectrometry information was exported and compared in the Human Metabolome database (HMDB) (<http://www.hmdb.ca/>) and Metlin database (<https://metlin.scripps.edu/>) to obtain specific information on metabolites.

The preprocessed data were uploaded to the MSG BioCloud platform (<https://cloud.majorbio.com>) for data analysis. The R package ropls (v1.6.2) was used for principal component analysis (PCA) and orthogonal least squares discriminant analysis (OPLS-DA). In addition, *t*-test and difference multiple analysis were performed. Differentially expressed metabolites between the *fliS*-RNAi and wild type groups were screened (VIP > 1, FDR < 0.05,  $|FC| \geq 1$ ), and the pathways involved in the differentially expressed metabolites were obtained using KEGG (<https://www.kegg.jp/kegg/pathway.html>). The Python software package SciPy was used for pathway enrichment analysis and Fisher's exact test was used to obtain the most relevant biological pathways.

## Combined analysis of transcriptomics and metabolomics

The VennDiagram package in R was used to analyze KEGG pathways involved in differentially expressed genes (DEGs) and differentially expressed metabolites. The top 10 KEGG pathways with the largest number of DEGs and differentially expressed metabolites were counted for visualization. The DEGs obtained by transcriptomics and differentially expressed metabolites obtained by metabolomics were integrated to analyze KEGG pathway data.

## Statistical analyses

All data are expressed as means ± standard deviation (SD) from at least three sets of independent experiments. Data analysis was implemented using IBM SPSS Statistics v22.0 (New York, USA), with one-way analysis of variance (ANOVA) with Dunnett's test used. *P*-values < 0.05 were considered statistically significant.

## Data access

The RNA-seq data were deposited in the GenBank SRA database under accession numbers SRP 374606 (*fliS*-RNAi strain infection group), SRP 370956 (NZBD9 strain infection group), and SRP 370960 (PBS injection group). The metabolome data were deposited in the China National GeneBank Database under accession number CNP0003231.

## Results

### Silencing efficiency of RNAi strains

The expression level of *fliS* in five different RNAi strains was verified by qRT-PCR. As shown in Figure 1A, all five shRNAs significantly reduced *fliS* mRNA expression by 64.2%, 76.7%, 89.0%, 77.7%, and 84.8%, respectively. Thus, five stably silenced strains of *P. plecoglossicida* were successfully constructed. Among them, the *fliS*-RNAi-126 strain (hereinafter the *fliS*-RNAi strain) showed the best RNAi effect and was selected for subsequent experiments (Figure 1A). As shown in Figure 1B, there were no significant differences in the growth curves of the *fliS*-RNAi and wild type strains.

### Effects of *fliS* silencing on *P. plecoglossicida* virulence-related characteristics

The LB agar plate-cultured colonies of the *fliS*-RNAi and wild type strains of *P. plecoglossicida* are shown in Figure 2A. Results indicated that the *fliS*-RNAi strain colonies were significantly smaller ( $6.58 \pm 0.11$  mm,  $p < 0.01$ ) than those of the wild type strain ( $8.37 \pm 0.08$  mm) (Figure 2B).

Biofilm formation of the *fliS*-RNAi and wild type strains of *P. plecoglossicida* is shown in Figure 2C. Compared to the wild type strain, the *fliS*-RNAi biofilm was lighter and deeper than that of LB. Results also showed that the OD<sub>590</sub> of *fliS*-RNAi was significantly lower ( $0.39 \pm 0.02$  nm,  $p < 0.001$ ) than that of the wild type strain ( $0.89 \pm 0.04$  nm) (Figure 2D).

Adhesion of the *fliS*-RNAi and wild type strains of *P. plecoglossicida* to the mucus surface of *E. coioides* is shown in Figure 2E. Results indicated that the adhesion ability of the *fliS*-RNAi strain was markedly weakened, with significantly fewer ( $286 \pm 6.20$  cells/vision,  $p < 0.001$ ) adhered bacteria compared to the wild type strain ( $814 \pm 22.20$  cells/vision) (Figure 2F).

Chemotaxis capacity of the *fliS*-RNAi and wild type strains of *P. plecoglossicida* is shown in Figure 2G. Results indicated that *fliS*-RNAi strain chemotaxis was marked weakened, with significantly lower ( $2.6 \times 10^4$  CFU/mL,  $p < 0.001$ ) chemotaxis compared to the wild type strain ( $4.7 \times 10^4$  CFU/mL).

### Effects of *fliS* silencing on *P. plecoglossicida* pathogenicity

The *E. coioides* infected with the wild type strain of *P. plecoglossicida* began to die at 2 dpi, with 100% mortality reached at 6 dpi. In contrast, no *E. coioides* infected with the *fliS*-RNAi strain died by 10 dpi, as also found in the PBS-injected controls (Figure 3A). Furthermore, the apparent characteristics of *E. coioides* spleens at 4 dpi (Figure 3B) showed many white nodules on the spleen surface of *E. coioides* infected by the wild type strain, but almost no white spots on the spleen surface of fish infected by the *fliS*-RNAi strain or PBS. As shown in Figure 3C, although pathogen load in the *fliS*-RNAi strain-infected *E. coioides* spleens did not change significantly from 1 dpi to 4 dpi, it was consistently significantly lower than that of the wild type strain, and relative pathogen load (*fliS*-RNAi strain pathogen load/wild type strain pathogen load) decreased sharply with the duration of infection. The *fliS* gene of both strains was more highly expressed in the spleen than *in vitro*, and *fliS*

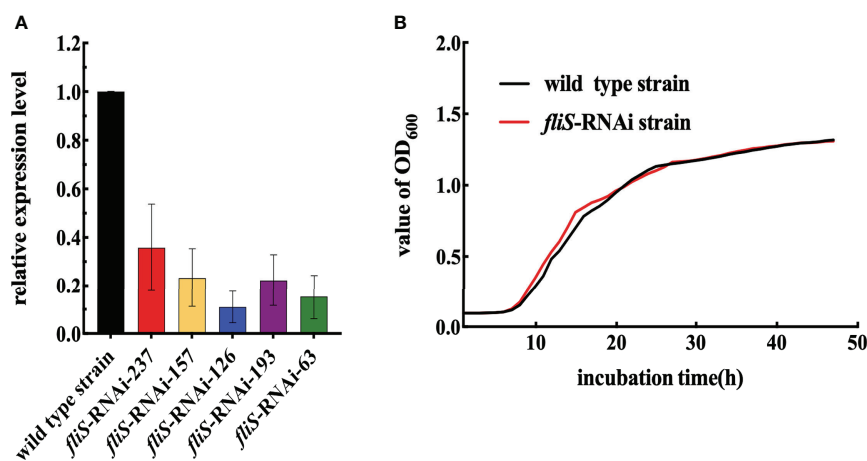


FIGURE 1  
Construction and growth curve of *P. plecoglossicida* *fliS*-RNAi strain. (A) *fliS* mRNA levels of *P. plecoglossicida* strains. (B) Growth curve of wild type and *fliS*-RNAi strains.

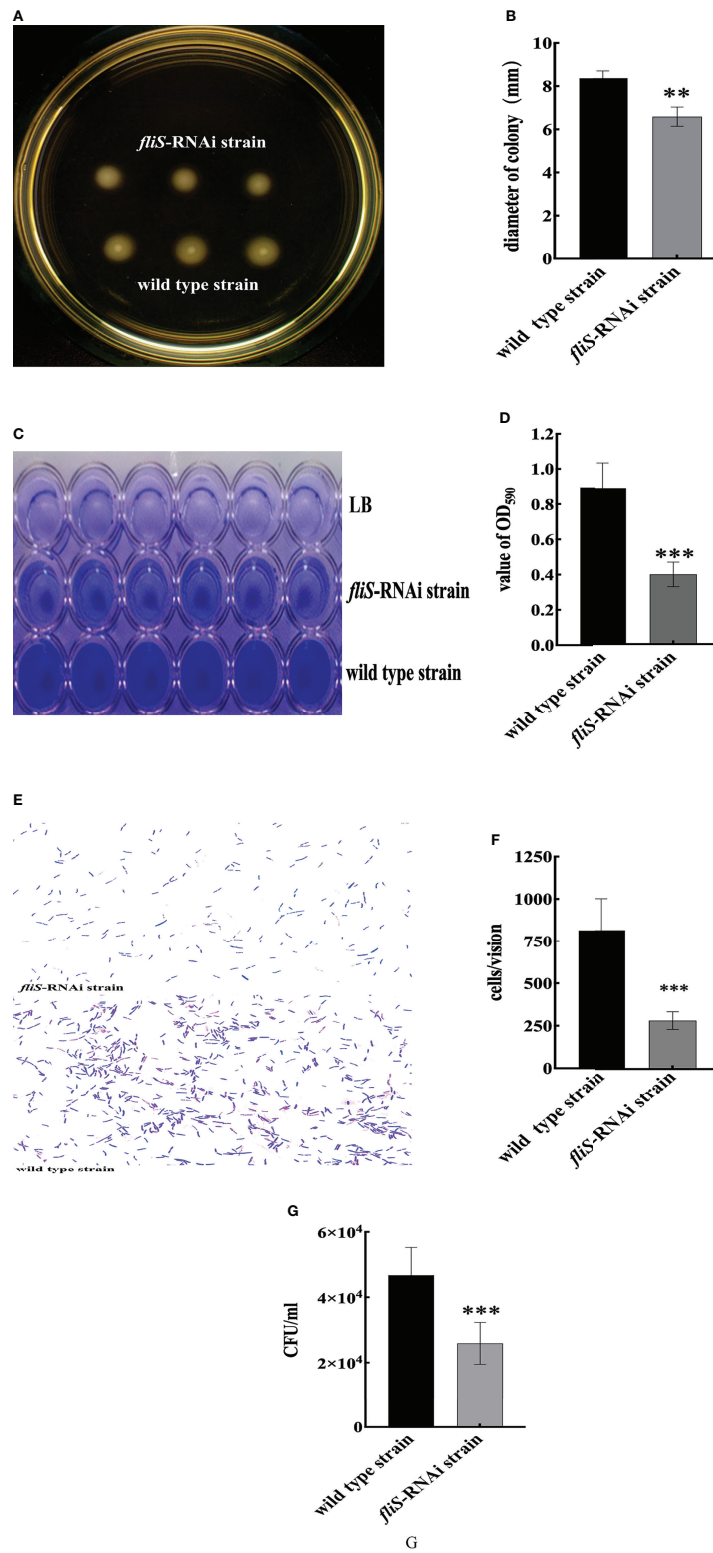


FIGURE 2

Characteristics of two *P. plecoglossida* strains. (A) Colonies of wild type and *fliS*-RNAi strain swarms on soft agar plates. (B) Colony diameters of wild type and *fliS*-RNAi strains. (C) Biofilm of wild type and *fliS*-RNAi strains. (D) Biofilm formation ability of wild type and *fliS*-RNAi strains. (E) Adhering bacteria under the microscope. (F) Adhesion ability of wild type and *fliS*-RNAi strains. (G) Chemotaxis capacity of wild type and *fliS*-RNAi strains. Data are mean ± SD. \**p* < 0.05, \*\**p* < 0.01, \*\*\**p* < 0.001.

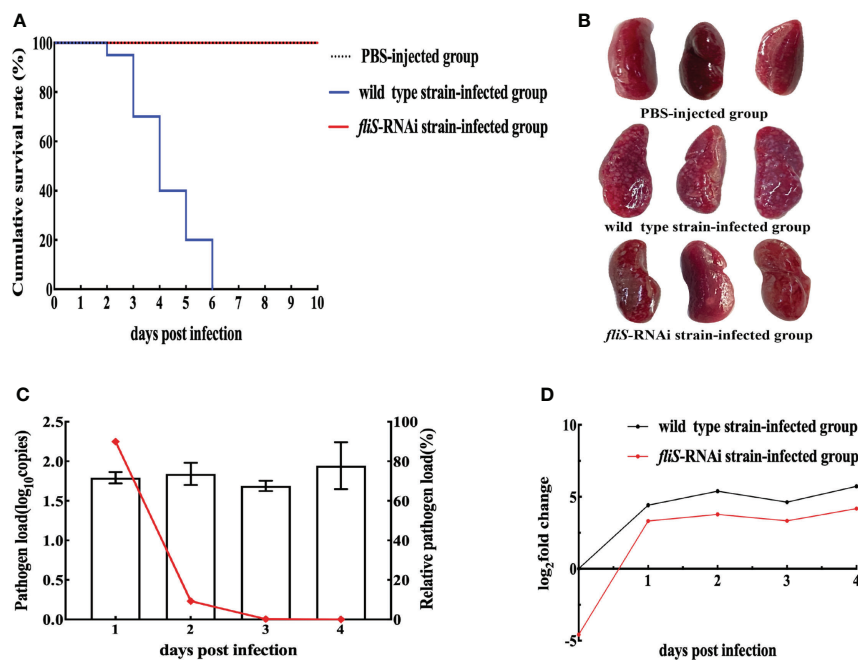


FIGURE 3

Pathogenicity of two *P. plecoglossicida* strains against *E. coioides*. (A) Survival rate. (B) Symptoms in *E. coioides* spleens at 4 dpi. (C) Pathogen load of *fliS*-RNAi strain in *E. coioides* spleens during infection. Column represents pathogen load in spleen, represented by copy number of housekeeping gene *gyrB*. Line graph represents relative pathogen load value (i.e., copy number of *gyrB* gene of *fliS*-RNAi strain/copy number of *gyrB* gene of wild type strain). (D) mRNA expression level of *fliS* gene of *P. plecoglossicida* in *E. coioides* spleens during infection.

expression in the *fliS*-RNAi strain was consistently lower than that in the wild type strain (Figure 3D).

## Effects of *fliS* silencing on infected *E. coioides* spleen transcriptome

RNA-seq was performed on the spleens of *E. coioides* infected with the *fliS*-RNAi or wild type strains of *P. plecoglossicida*. Quality control of the original sequencing data showed that the Q20 (percentage of bases with quality value  $\geq 20$ ) of each sample was above 97.41%, Q30 (percentage of bases with quality value  $\geq 30$ ) was above 93.94%, and GC content was about 50% (Supplementary Table 4). The sequencing error rate was less than 0.1%, and sequencing accuracy was high. Thus, the quality of the sequencing data met the requirements for subsequent data processing and analysis.

Through the correlation analysis between biological repeat samples, on the one hand to test whether the variation between biological repeats meets the expectations of experimental design, on the other hand to provide basic reference for DEG analysis. Pearson correlation analysis was used to assess the associations between the wild type strain-infected group and *fliS*-RNAi strain-infected groups. The minimum and maximum Pearson

correlation coefficients between groups were 0.098 and 0.164, respectively, and within groups were 0.99 and 1, respectively (Supplementary Figure 1). Thus, biological repeatability was deemed good, with strong intra-group correlation and small inter-group correlation. The experimental data were therefore reliable and could be used for further analysis of DEGs.

EdgeR was used for differential transcript analysis of *E. coioides*. The statistical standard of mRNA expression level of transcriptome data was  $FDR < 0.05$  and  $|\log_2 FC| \geq 1$  as GO and KEGG pathway enrichment analysis of DEGs. Transcriptomic analysis of *E. coioides* spleens sampled at 4 dpi identified 52 006 DEGs between the *fliS*-RNAi and wild type strain-infected spleens, including 38 393 up-regulated DEGs and 13 613 down-regulated DEGs (Figure 4A). The top 50 most significantly up-regulated and down-regulated DEGs were selected for analysis (Figure 4B).

Figure 4C shows the top 20 GO enrichment results. Based on GO functional annotation, the DEGs were annotated into three categories, i.e., biological process (BP), cell composition (CC), and molecular function (MF), with significant enrichment in protein-containing complex and immune system process and response to stimulus.

Further enrichment analysis identified 23 KEGG pathways involved in the immune response (Figure 4D), with 23.8% of

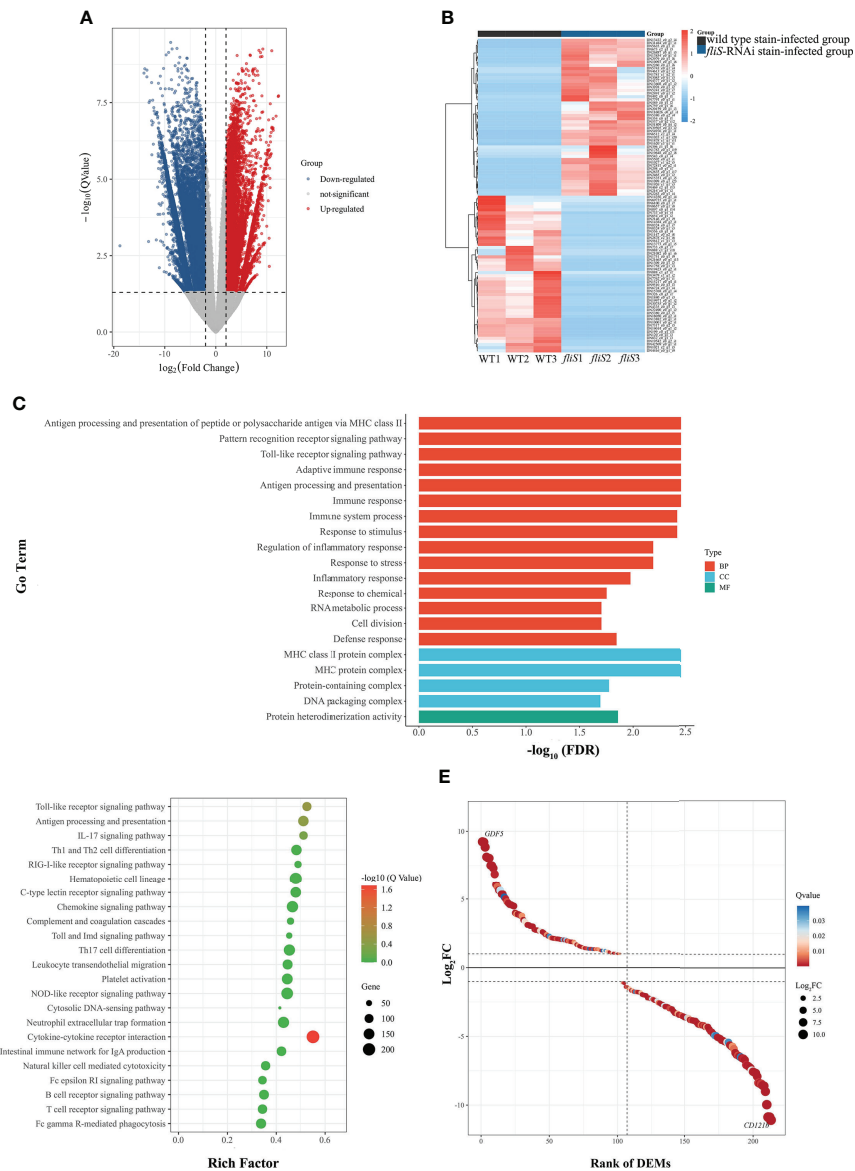


**FIGURE 4** Comparative transcriptomic analysis of *E. coioides* spleens infected by *fliS*-RNAi and wild type strains of *P. plecoglossida*. **(A)** Volcano plot obtained from EdgeR analysis. **(B)** Heat map of top 50 up-regulated (red) and down-regulated DEGs (blue). Deeper color indicates higher expression difference. **(C)** GO enrichment analysis of DEGs. **(D)** KEGG pathway enrichment analysis of DEGs. **(E)** Expression level of DEGs in cytokine-cytokine receptor interaction pathway.

DEGs enriched in immune system pathways. Based on Fisher’s exact test, 213 DEGs were significantly enriched in the cytokine-cytokine receptor interaction pathway, including 102 significantly up-regulated DEGs and 111 significantly down-regulated DEGs (Figure 4E). Most genes involved in this pathway were chemokines, including class I helical cytokines, class II helical cytokines, IL1-like cytokines, IL17-like cytokines, TNF family, and TGF-β family. Notably,

chemokines such as *CXCL8*, *CXCR2*, *CCL11*, and *CXCL12* were up-regulated, while certain inflammatory genes such as *IL1B*, *IL1R2*, *IL17*, and *IL17RA* were down-regulated. Furthermore, *TNF* gene expression was down-regulated, while *TGFB1* and *TGFB2* gene expression levels were up-regulated. qRT-PCR verification was performed on 10 randomly selected DEGs from the RNA-seq database. Results showed that the expression trends of the selected DEGs were

consistent with those of transcriptome sequencing (Supplementary Figure 2).

## Effects of *fliS* silencing on infected *E. coioides* spleen metabolome

To determine the cumulative differences in spleen metabolites between the *fliS*-RNAi and wild type strain-infected groups, PCA was performed to obtain scores of the two principal components. In the total ion PCA model, PC1 = 60.30%, PC2 = 8.52% (Figure 5A),  $R^2X = 0.603$ , and the cumulative difference explanatory value was greater than 0.5, so the established PCA model was stable and could be used for subsequent metabolic difference analysis. To display the metabolic differences between the two groups more accurately, the supervised OPLS-DA model was used for further analysis. The *fliS*-RNAi strain-infected samples were mainly distributed in the negative half of PC1, while the wild type strain-infected samples were mainly distributed in the positive half of PC1, so the model could effectively distinguish the two groups of samples (Figure 5B). The replacement test of OPLS-DA model showed that  $R^2X$  and  $R^2Y$  were 0.753 and 0.991, and  $Q^2$  was 0.986, which were close to 1 and had good reliability (Supplementary Table 5).

The differentially expressed metabolites between the two infection groups were analyzed. Based on screening criteria (FDR < 0.05, VIP > 1, FC > 1, FC < 1), 326 differentially expressed metabolites were identified, mainly divided into organic acids, lipids, carbohydrates, nucleic acids, peptides, vitamins and coenzyme factors, steroids, hormones and transmission media, and antibiotics according to their biological function. Compared with the wild type strain-infected group, 107 and 219 differentially expressed metabolites in the *fliS*-RNAi strain-infected group were up-regulated (FC > 1) and down-regulated (FC < 1), respectively (Figure 5C). The top 20 up-regulated and down-regulated differentially expressed metabolites were selected for further analysis (Figure 5D).

Based on KEGG pathway enrichment analysis, 105 metabolic pathways were annotated, with 18 found to be significantly enriched ( $P < 0.05$ ), including glycosylphosphatidylinositol (GPI)-anchor biosynthesis, glycerophospholipid metabolism, arginine biosynthesis, arginine and proline metabolism, ABC transporters, linoleic acid metabolism, alpha-linolenic acid metabolism, sphingolipid signaling pathway, and glutathione metabolism. Six metabolic pathways were highly significantly enriched ( $P < 0.01$ ), including linoleic acid metabolism, arginine and proline metabolism, glycerophospholipid metabolism, choline metabolism in cancer, purine metabolism, and especially arginine biosynthesis pathway (Figure 5E).

## Comprehensive transcriptomic and metabolomic analysis

The transcriptomic and metabolomic results were correlated. Venn analysis indicated that 101 KEGG pathways were shared between the transcriptomes and metabolomes, accounting for 94.2% of the total metabolome pathways (105) and 29.1% of the total transcriptome pathways (347) (Figure 6A). Figure 6B shows the top 10 KEGG pathways with the largest number of DEGs and differentially expressed metabolites. We found that arginine biosynthesis pathway was most involved (Figure 6B), and the correlation between metabolites and DEGs was the best (Figure 6C). So focused on this pathway to explore the relationship between them, further in-depth analysis was conducted.

We identified 11 DEGs and seven differentially expressed metabolites involved in the arginine biosynthesis pathway (Figure 6D). Among them, *glnA* and *argH* were up-regulated and *glsA* and *rocF* were down-regulated, while glutamine and arginine were up-regulated and ornithine and citrulline were down-regulated. We found that *glnA* gene and *argH* gene in the transcriptome involved in arginine biosynthesis pathway, as well as glutamine and arginine in the metabolic group were significantly up-regulated. Among them, *glnA* gene was positively regulated with glutamine, and *argH* gene was positively regulated with arginine.

## Discussion

RNAi technology is a highly efficient tool for investigating gene function (Dai et al., 2005; Fellmann et al., 2011; Liu et al., 2020). In this study, the five shRNAs used showed different *fliS* silencing efficiency, indicating the versatility of RNAi and differences at different sites. Stable and efficient silencing is essential for gene function studies. Here, the best *fliS* silencing efficiency obtained was 89%, and the effect persisted at all sampling times, thus laying the foundation for this research.

Motility mediated by the bacterial flagellar system increases the probability of contact, adhesion, and colonization of host cells, thus highlighting the critical role of flagella in the infection process (Houry et al., 2010; Chaban et al., 2015). Flagella are also involved in many other processes, including chemotaxis, biofilm formation, virulence factor secretion, and eukaryotic immune system regulation (Duan et al., 2013; Gallego-Hernandez et al., 2020). Here, *fliS* gene silencing significantly reduced *P. plecoglossicida* motility, biofilm formation, and adhesion ability, which are factors closely related to bacterial pathogenicity (Song et al., 2019; Zhang et al., 2020). We previously found that the *P. plecoglossicida fliM* gene was involved in flagellar assembly (Sun et al., 2019) and the *fliG*

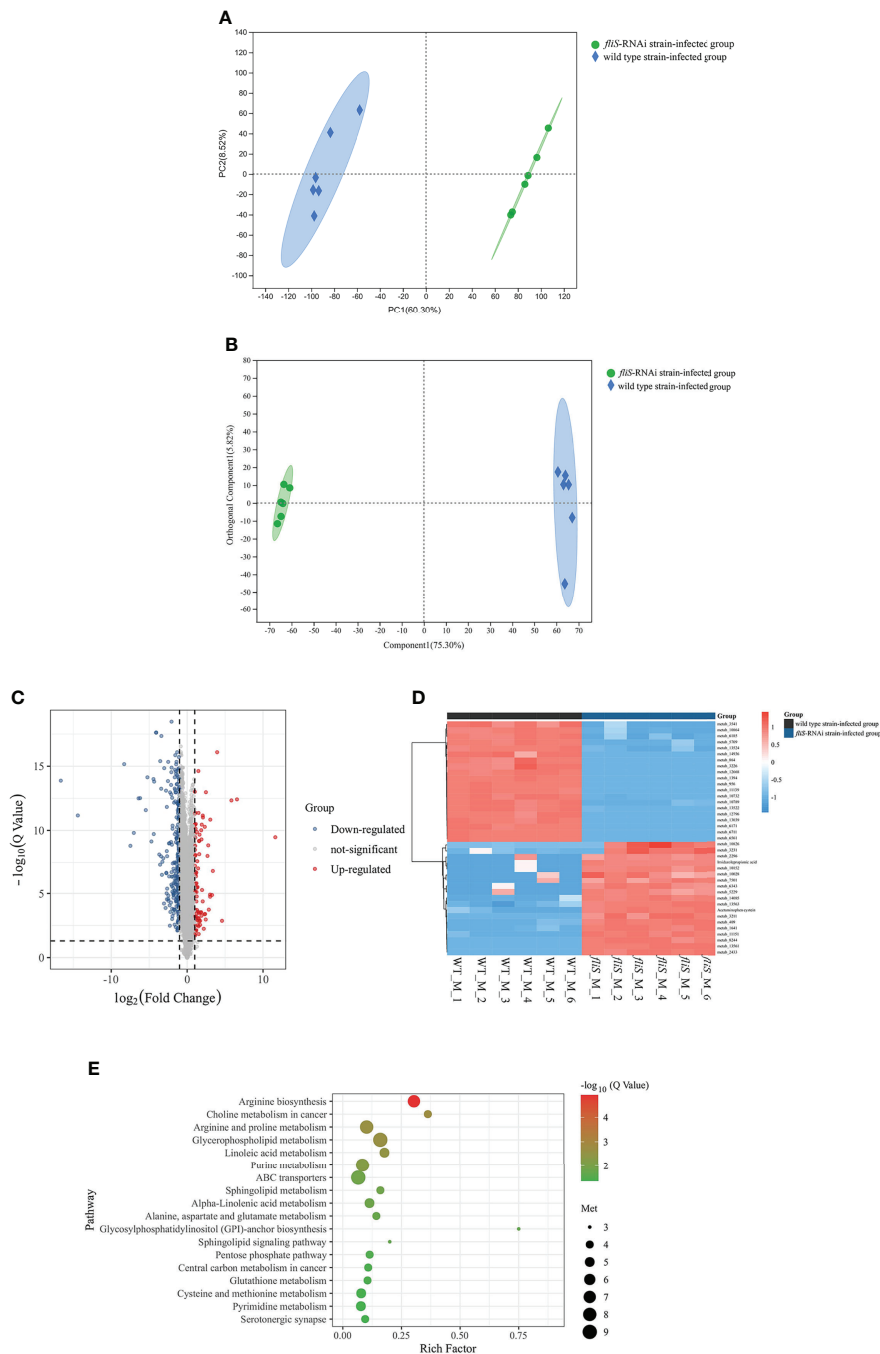


**FIGURE 5**  
 Comparative metabolomic analysis of *E. cooides* spleens infected by *fliS*-RNAi and wild type strains of *P. plecoglossida*. **(A)** PCA diagram. X-axis shows first principal component, Y-axis shows second principal component. **(B)** OPLS-DA score plot. Component 1 represents first predictive principal component interpretation and Orthogonal Component 1 represents first orthogonal component interpretation. **(C)** Volcano plot of differentially expressed metabolites. **(D)** Heat map comparison of differentially expressed metabolites. **(E)** KEGG enrichment of differentially expressed metabolites.



regulated DEGs. These findings indicated that *fliS* gene silencing significantly affected transcription in infected *E. coioides*.

Based on GO and KEGG pathway enrichment analysis of the 52006 DEGs, 23 immune-related pathways were enriched, especially the cytokine-cytokine receptor interaction pathway. Thus, *fliS* gene silencing significantly affected the immune response of *P. plecoglossicida*-infected *E. coioides*.

Cytokines are small molecular polypeptides or glycoproteins synthesized and secreted by a variety of tissue cells (mainly immune cells) (Wang et al., 2020; Chauhan et al., 2021), which regulate cell growth, differentiation, and immune response (Curfs et al., 1997). In this study, compared with the control group, *IL-1B* gene expression was significantly down-regulated in the spleens of *E. coioides* infected with the *fliS*-RNAi strain, with down-regulation also observed for the receptor gene *IL1R2* and downstream gene *TNF*. The *IL-1B* gene encodes IL-1 $\beta$ , which can activate the release of other pro-inflammatory cytokines, such as TNF, in response to viral and bacterial stimulation (Eder, 2009; Fathy et al., 2019; Ren and Torres, 2009; Zhang et al., 2022). IL-1 $\beta$  also plays a key role in inflammation and immune response, with important implications in disease pathogenesis (Lukens et al., 2012). When fish are stimulated by bacteria, viruses, endotoxins, and other pathogenic factors, the transcription of IL-1 $\beta$  is significantly up-regulated in immune organs, skin, gills, intestines, and other tissues (Yang et al., 2017; Dong et al., 2021; Tian et al., 2021). In this study, the significant down-regulation of *IL-1B* in the *fliS*-RNAi strain-infected *E. coioides* spleens indicated a milder inflammatory response compared to those fish infected with the wild type strain, consistent with the lower pathogen load in the *fliS*-RNAi-infected spleens.

Our results also showed that *TGFB1* and *TGFB2* were up-regulated in the *fliS*-RNAi strain-infected *E. coioides* spleens compared with the wild type-infected group. *TGFB1* and *TGFB2* encode TGF- $\beta$ , a multifunctional cytokine involved in immune response regulation (Haque and Morris, 2017), and play an important role in cell growth, proliferation, differentiation, adhesion, migration, polarization of Th17 reaction, generation, and apoptosis of reactive oxygen species (Morikawa et al., 2016; Seoane and Gomis, 2017; Wang et al., 2019). In the present study, up-regulation of *TGFB1* and *TGFB2* indicated that *E. coioides* infected with the *fliS*-RNAi strain showed a stronger TGF- $\beta$ -based immune response than *E. coioides* infected with the wild type strain of *P. plecoglossicida*. Furthermore, *E. coioides* exhibited different inflammatory and TGF- $\beta$ -based immune responses to infection by the wild type and *fliS*-RNAi strains of *P. plecoglossicida*, indicating complexity of the immune response.

Metabolomic analysis revealed significantly different patterns in the *E. coioides* infected with the wild type and *fliS*-RNAi strains. These results suggest that *fliS* gene silencing can significantly alter the metabolic pattern of *E. coioides* under *P. plecoglossicida* infection, consistent with the changes in the transcription of *E. coioides* infected with the two strains of *P. plecoglossicida*.

Combined with metabolomic analysis, our results showed that the differentially expressed metabolites were mainly concentrated in the arginine and proline metabolism, arginine biosynthesis, glutathione metabolism, and other metabolic pathways. Arginine biosynthesis was the most significantly enriched KEGG pathway. Seven differentially expressed metabolites were enriched in this pathway, including L-arginine and L-glutamine, which were significantly up-regulated. Amino acid metabolism plays an important role in the immune system to fight pathogen infection (Synne et al., 2016). The arginine biosynthesis pathway, including arginine, glutamine, and other metabolites, is involved in oxidative stress, biofilm formation, immune response, and inflammatory response (Wang et al., 2021; Huang et al., 2022; Long et al., 2022). In addition, arginine biosynthesis is a key metabolic pathway for the antitumor effects of drugs, with the arginine metabolite playing an important role (Chen et al., 2021). Previous research has shown that the survival rate of *Aeromonas hydrophila*-infected Jian carp (*Cyprinus carpio* var. Jian) significantly increases after arginine feeding, and arginine can enhance immunity and disease resistance (Chen et al., 2015). In addition, arginine regulates mRNA expression of the TOR pathway, as well as inflammatory cytokines and antioxidant-related signaling molecules (Habte-Tsion, 2020). Inhibition of the TOR pathway significantly hinders the arginine enzyme metabolism and Arg-NO metabolism pathways and improves humoral and cellular immunity (Habte-Tsion, 2020). In this study, we found that L-arginine was up-regulated in the spleens of *E. coioides* infected with the *fliS*-RNAi strain compared to the wild type strain, suggesting that virulence of the silenced strain was weakened, while the L-arginine metabolic pathway was strengthened, resulting in an enhanced immune response.

Similarly, studies have shown that dietary probiotics can improve L-glutamine content in *Litopenaeus vannamei*, thereby regulating the immune response (Chien et al., 2020). In *Oreochromis niloticus*, glutamine supplementation can enhance the bactericidal ability of *Streptococcus* through macrophages (Carvalho et al., 2018). In *Scophthalmus maximus*, glutamine can reduce the negative effects of soybean meal on intestinal immune function by increasing intestinal immune components and reducing intestinal inflammation (Gu et al., 2017). In this study, we found that glutamine levels were up-regulated in the spleens of *E. coioides* infected with the *fliS*-RNAi strain compared to those infected with the wild type strain. This may be due to stimulation of *P. plecoglossicida*, L-glutamine needs to be consumed by many immune cells, thereby increasing its synthesis to facilitate further immune response.

We speculate that infection with the *fliS*-RNAi strain of *P. plecoglossicida* may induce arginine biosynthesis pathway expression in *E. coioides*, which may help prevent pathogen infection, thereby weakening *P. plecoglossicida* damage to the host.

## Conclusions

Our study showed that the *fliS* gene is involved in the regulation of *P. plecoglossicida* motility, adhesion, and biofilm formation, and may be a virulence gene of *P. plecoglossicida*. Silencing the *fliS* gene significantly affected the transcriptome and metabolome of the *E. coioides* spleen following *P. plecoglossicida* infection. The cytokine-cytokine receptor interaction pathway was the most significantly enriched immune-related pathway in the transcriptome, while the arginine biosynthesis pathway was the most significantly enriched pathway in the metabolome. The transcriptome and metabolome changes indicated that the inflammatory response of *E. coioides* infected with the *fliS*-RNAi strain was milder than that infected with the wild type strain.

## Data availability statement

The RNA-seq data were deposited in the GenBank SRA database under accession numbers SRP 374606 (*fliS*-RNAi strain infection group), SRP 370956 (NZBD9 strain infection group), and SRP 370960 (PBS injection group). The metabolome data were deposited in the China National GeneBank Database under accession number CNP0003231.

## Ethics statement

The animal protocols were approved by the Animal Ethics Committee of Jimei University (Acceptance NO JMULAC201159).

## Author contributions

Seven authors contributed to the article, QY conceived the experiments. WW and LZ conducted the experiments. All authors assisted in the collection and interpretation of data.

## References

- Borrego, J., Valverde, E., Labella, A., and Castro, D. (2017). Lymphocystis disease virus: its importance in aquaculture. *Rev. Aquac.* 9 (2), 179–193. doi: 10.1111/raq.12131
- Cai, S., Cheng, H., Pang, H., and Jian, J. (2017). Role of the *toxR* gene from fish pathogen *Vibrio alginolyticus* in the physiology and virulence. *Indian J. Microbiol.* 57 (4), 477–484. doi: 10.1007/s12088-017-0685-x
- Carvalho, P., Yamamoto, F., Barros, M., and Gatlin Iii, D. (2018). L-glutamine *in vitro* supplementation enhances Nile tilapia *Oreochromis niloticus* (Linnaeus 1758) leukocyte function. *Fish Shellfish Immunol.* 80, 592–599. doi: 10.1016/j.fsi.2018.06.043
- Chaban, B., Hughes, H. V., and Beeby, M. (2015). The flagellum in bacterial pathogens: For motility and a whole lot more. *Semin. Cell Dev. Biol.* 46, 91–103. doi: 10.1016/j.semcdb.2015.10.032

WW and QY wrote the manuscript. All authors contributed to the article and approved the submitted version.

## Funding

This work was supported by the Natural Science Foundation of Fujian Province under contract No. 2021J01828, National Natural Science Foundation of China under contract No. 31972836, open fund of Fujian Province Key Laboratory of Special Aquatic Formula Feed under contract No. TMKJZ2101.

## Conflict of interest

Authors JNZ and JLZ were employed by Fujian Tianma Technology Company Limited, Fuzhou, China.

The remaining authors declare that the research was conducted in the absence of any commercial or financial relationships that could be construed as a potential conflict of interest.

## Publisher's note

All claims expressed in this article are solely those of the authors and do not necessarily represent those of their affiliated organizations, or those of the publisher, the editors and the reviewers. Any product that may be evaluated in this article, or claim that may be made by its manufacturer, is not guaranteed or endorsed by the publisher.

## Supplementary material

The Supplementary Material for this article can be found online at: <https://www.frontiersin.org/articles/10.3389/fmars.2022.987825/full#supplementary-material>

- metabolism and hexosamine biosynthetic pathway. *Fish Shellfish Immunol.* 98, 176–185. doi: 10.1016/j.fsi.2020.01.014
- Condry, D., and Nilles, M. (2017). Introduction to type III secretion systems. *Methods Mol. Biol.* 1531, 1–10. doi: 10.1007/978-1-4939-6649-3\_1
- Curfs, J., Meis, J., and Hoogkamp-korstanje, J. (1997). A primer on cytokines: Sources, receptors, effects, and inducers. *Clin. Microbiol. Rev.* 10 (4), 742–780. doi: 10.1128/CMR.10.4.742
- Dai, F., Yusuf, F., Farjah, G., and Brand-Saberi, B. (2005). RNAi-induced targeted silencing of developmental control genes during chicken embryogenesis. *Dev. Biol.* 285 (1), 80–90. doi: 10.1016/j.ydbio.2005.06.005
- Diao, J., Liu, H., Hu, F., Li, L., Wang, X., Gai, C., et al. (2019). Transcriptome analysis of immune response in fat greenling (*Hexagrammos otakii*) against *Vibrio harveyi* infection. *Fish Shellfish Immunol.* 84, 937–947. doi: 10.1016/j.fsi.2018.10.067
- Dong, W., Gao, W., Cui, J., and Sun, Y. (2021). microRNA-148 is involved in NF- $\kappa$ B signaling pathway regulation after LPS stimulation by targeting IL-1 $\beta$  in miyu croaker. *Fish Shellfish Immunol.* 118, 66–71. doi: 10.1016/j.fsi.2021.08.028
- Duan, Q., Zhou, M., Zhu, L., and Zhu, G. (2013). Flagella and bacterial pathogenicity. *J. Basic Microbiol.* 53 (1), 1–8. doi: 10.1002/jobm.201100335
- Eder, C. (2009). Mechanisms of interleukin-1 $\beta$  release. *Immunobiology* 214 (7), 543–553. doi: 10.1016/j.imbio.2008.11.007
- Fathy, S., Mohamed, M., Ali, M., and Alattar, A. (2019). Influence of *IL-6*, *IL-10*, *IFN- $\gamma$*  and *TNF- $\alpha$*  genetic variants on susceptibility to diabetic kidney disease in type 2 diabetes mellitus patients. *Biomarkers* 24 (1), 43–55. doi: 10.1080/1354750X.2018.1501761
- Fellmann, C., Zuber, J., McJunkin, K., Chang, K., Malone, C., Dickins, R., et al. (2011). Functional identification of optimized RNAi triggers using a massively parallel sensor assay. *Mol. Cell* 41 (6), 733–746. doi: 10.1016/j.molcel.2011.02.008
- Gallego-Hernandez, A., DePas, W., Park, J., Teschler, J., Hartmann, R., Jeckel, H., et al. (2020). Upregulation of virulence genes promotes *Vibrio cholerae* biofilm hyperinfectivity. *Proc. Natl. Acad. Sci. U.S.A.* 117 (20), 11010–11017. doi: 10.1073/pnas.1916571117
- Gu, H. (2017). Role of flagella in the pathogenesis of *Helicobacter pylori*. *Curr. Microbiol.* 74 (7), 863–869. doi: 10.1007/s00284-017-1256-4
- Gu, M., Bai, N., Xu, B., and Zhang, Z. (2017). Protective effect of glutamine and arginine against soybean meal-induced enteritis in the juvenile turbot (*Scophthalmus maximus*). *Fish Shellfish Immunol.* 70, 95–105. doi: 10.1016/j.fsi.2017.08.048
- Habte-Tsion, H. (2020). A review on fish immuno-nutritional response to indispensable amino acids in relation to TOR, NF- $\kappa$ B and Nrf2 signaling pathways: Trends and prospects. *Comp. Biochem. Physiol. B Biochem. Mol. Biol.* 241, 110389. doi: 10.1016/j.cbpb.2019.110389
- Haque, S., and Morris, J. (2017). Transforming growth factor- $\beta$ : A therapeutic target for cancer. *Hum. Vaccin Immunother.* 13 (8), 1741–1750. doi: 10.1080/21645515.2017.1327107
- He, L., Wang, L., Zhao, L., Zhuang, Z., Wang, X., Huang, H., et al. (2021). Integration of RNA-seq and RNAi reveals the contribution of *znuA* gene to the pathogenicity of *Pseudomonas plecoglossicida* and to the immune response of *Epinephelus coioides*. *J. Fish Dis.* 44, 1831–1841. doi: 10.1111/jfd.13502
- Houry, A., Briandet, R., Aymerich, S., and Gohar, M. (2010). Involvement of motility and flagella in *Bacillus cereus* biofilm formation. *Microbiol. (Reading)* 156 (Pt 4), 1009–1018. doi: 10.1099/mic.0.034827-0
- Huang, L., He, X., Peng, W., He, X., Xu, B., Xu, H., et al. (2022). Hyperuricemia induces liver injury by upregulating HIF-1 $\alpha$  and inhibiting arginine biosynthesis pathway in mouse liver and human L02 hepatocytes. *Biochem. Biophys. Res. Commun.* 617, 55–61. doi: 10.1016/j.bbrc.2022.05.096
- Jiao, J., Zhao, L., Huang, L., Qin, Y., Su, Y., Zheng, W., et al. (2021). The contributions of *fliG* gene to the pathogenicity of *Pseudomonas plecoglossicida* and pathogen-host interactions with *Epinephelus coioides*. *Fish Shellfish Immunol.* 119, 238–248. doi: 10.1016/j.fsi.2021.09.03
- Lertsethtakarn, P., Ottemann, K., and Hendrixson, D. (2011). Motility and chemotaxis in *Campylobacter* and *Helicobacter*. *Annu. Rev. Microbiol.* 65, 389–410. doi: 10.1146/annurev-micro-090110-102908
- Liu, Z., Zhao, L., Huang, L., Qin, Y., Zhang, J., Zhang, J., et al. (2020). Integration of RNA-seq and RNAi provides a novel insight into the immune responses of *Epinephelus coioides* to the *impB* gene of *Pseudomonas plecoglossicida*. *Fish Shellfish Immunol.* 105, 135–143. doi: 10.1016/j.fsi.2020.06.023
- Li, C., Wang, S., Ren, Q., He, T., and Chen, X. (2020). An outbreak of visceral white nodules disease caused by *Pseudomonas plecoglossicida* at a water temperature of 12 degrees c in cultured large yellow croaker (*Larimichthys crocea*) in China. *J. Fish Dis.* 43 (11), 1353–1361. doi: 10.1111/jfd.13206
- Long, S., Dong, X., Liu, H., Yan, X., Tan, B., Zhang, S., et al. (2022). Effect of dietary oxidized fish oil on liver function in hybrid grouper ( $\varnothing$  *Epinephelus fuscoguttatus*  $\times$   $\delta$  *Epinephelus lanceolatus*). *Aquac. Rep.* 22, 101000. doi: 10.1016/j.aqrep.2021.101000
- Lowenthal, A., Hill, M., Sycuro, L., Mehmood, K., Salama, N., Ottemann, K., et al. (2009). Functional analysis of the *Helicobacter pylori* flagellar switch proteins. *J. Bacteriol.* 191 (23), 7147–7156. doi: 10.1128/JB.00749-09
- Lukens, J., Gross, J., and Kanneganti, T. (2012). IL-1 family cytokines trigger sterile inflammatory disease. *Front. Immunol.* 3, 315. doi: 10.3389/fimmu.2012.00315
- Luo, G., Sun, Y., Huang, L., Su, Y., Zhao, L., Qin, Y., et al. (2020). Time-resolved dual RNA-seq of tissue uncovers *Pseudomonas plecoglossicida* key virulence genes in host-pathogen interaction with *Epinephelus coioides*. *Environ. Microbiol.* 22 (2), 677–693. doi: 10.1111/1462-2920.14884
- Luo, G., Zhao, L., Xu, X., Qin, Y., Huang, L., Su, Y., et al. (2019). Integrated dual RNA-seq and dual iTRAQ of infected tissue reveals the functions of a diguanylate cyclase gene of *Pseudomonas plecoglossicida* in host-pathogen interactions with *Epinephelus coioides*. *Fish Shellfish Immunol.* 95, 481–490. doi: 10.1016/j.fsi.2019.11.008
- Mao, L., Qin, Y., Kang, J., Wu, B., Huang, L., Wang, S., et al. (2020). Role of LuxR-type regulators in fish pathogenic *Aeromonas hydrophila*. *J. Fish Dis.* 43 (2), 215–225. doi: 10.1111/jfd.13114
- Miao, E., Mao, D., Yudkovsky, N., Bonneau, R., Lorang, C., Warren, S., et al. (2010). Innate immune detection of the type III secretion apparatus through the NLR4 inflammasome. *Proc. Natl. Acad. Sci. U.S.A.* 107 (7), 3076–3080. doi: 10.1073/pnas.0913087107
- Morikawa, M., Derynck, R., and Miyazono, K. (2016). TGF- $\beta$  and the TGF- $\beta$  family: Context-dependent roles in cell and tissue physiology. *Cold Spring Harb. Perspect. Biol.* 8 (5), a021873. doi: 10.1101/cshperspect.a021873
- Mugimba, K., Byarugaba, D., Mutoloki, S., Evensen, O., and Munang'andu, H. (2021). Challenges and solutions to viral diseases of finfish in marine aquaculture. *Pathogens* 10 (6), 673. doi: 10.3390/pathogens10060673
- Muskotal, A., Kiraly, R., Sebestyén, A., Gugolya, Z., Vegh, B., Vonderviszt, F., et al. (2006). Interaction of FliS flagellar chaperone with flagellin. *FEBS Lett.* 580 (16), 3916–3920. doi: 10.1016/j.febslet.2006.06.024
- Nishimori, E., Kita-Tsukamoto, K., and Wakabayashi, H. (2000). *Pseudomonas plecoglossicida* sp. nov., the causative agent of bacterial haemorrhagic ascites of ayu, *Plecoglossus altivelis*. *Int. J. Syst. Evol. Microbiol.* 50 (1), 83–89. doi: 10.1099/00207713-50-1-83
- Ozin, A., Claret, L., Auvray, F., and Hughes, C. (2003). The FliS chaperone selectively binds the disordered flagellin c-terminal D0 domain central to polymerisation. *FEMS Microbiol. Lett.* 219 (2), 219–224. doi: 10.1016/s0378-1097(02)01208-9
- Radomska, K., Wosten, M., Ordonez, S., and van Putten, J. (2017). Importance of *Campylobacter jejuni* FliS and FliW in flagella biogenesis and flagellin secretion. *Front. Microbiol.* 8, 1060. doi: 10.3389/fmicb.2017.01060
- Ren, K., and Torres, R. (2009). Role of interleukin-1 $\beta$  during pain and inflammation. *Brain Res. Rev.* 60 (1), 57–64. doi: 10.1016/j.brainresrev.2008.12.020
- Seoane, J., and Gomis, R. (2017). TGF- $\beta$  family signaling in tumor suppression and cancer progression. *Cold Spring Harb. Perspect. Biol.* 9 (12), a022277. doi: 10.1101/cshperspect.a022277
- Song, H., Kang, Y., Zhang, D., Chen, L., Qian, A., Shan, X., et al. (2019). Great effect of porin(aha) in bacterial adhesion and virulence regulation in *Aeromonas veronii*. *Microbial. Pathog.* 126, 269–278. doi: 10.1016/j.micpath.2018.11.002
- Sun, Y., Zhuang, Z., Wang, X., Huang, H., Fu, Q., Yan, Q., et al. (2019). Dual RNA-seq reveals the effect of the *flgM* gene of *Pseudomonas plecoglossicida* on the immune response of *Epinephelus coioides*. *Fish Shellfish Immunol.* 87, 515–523. doi: 10.1016/j.fsi.2019.01.041
- Synne, M., Rune, W., and Marit, E. (2016). Functional amino acids in fish health and welfare. *Front. Biosci.* 8 (1), 143–169. doi: 10.2741/757
- Tang, Y., Jiao, J., Zhao, L., Zhuang, Z., Wang, X., Fu, Q., et al. (2022). The contribution of *exbB* gene to pathogenicity of *Pseudomonas plecoglossicida* and its interactions with *Epinephelus coioides*. *Fish Shellfish Immunol.* 120, 610–619. doi: 10.1016/j.fsi.2021.12.026
- Tang, Y., Xin, G., Zhao, L., Huang, L., Qin, Y., Su, Y., et al. (2020). Novel insights into host-pathogen interactions of large yellow croakers (*Larimichthys crocea*) and pathogenic bacterium *Pseudomonas plecoglossicida* using time-resolved dual RNA-seq of infected spleens. *Zool. Res.* 41 (3), 314–327. doi: 10.24272/zj.zissn.2095-8137.2020.035
- Tian, G., Xie, M., Wang, B., Gao, W., Yuan, H., Wei, H., et al. (2021). Identification and expression of IL-1 $\beta$  in the endangered dabry's sturgeon (*Acipenser dabryanus*). *Aquac. Rep.* 20, 100698. doi: 10.1016/j.aqrep.2021.100698
- Wang, N., Gao, J., Yuan, L., Jin, Y., and He, G. (2021). Metabolomics profiling during biofilm development of *Bacillus licheniformis* isolated from milk powder. *Int. J. Food Microbiol.* 337, 108939. doi: 10.1016/j.ijfoodmicro.2020.108939

- Wang, L. Y., Liu, Z. X., Zhao, L. M., Huang, L., Qin, Y., Su, Y., et al. (2020). Dual RNA-seq provides novel insight into the roles of *dksA* from *Pseudomonas plecoglossicida* in pathogen-host interactions with large yellow croakers (*Larimichthys crocea*). *Zool. Res.* 41 (4), 410–422. doi: 10.24272/j.zissn.2095-8137.2020.048
- Wang, Y., Wang, X., Ali, F., Li, Z., Fu, Y., Yang, X., et al. (2019). Comparative extracellular proteomics of *Aeromonas hydrophila* reveals iron-regulated secreted proteins as potential vaccine candidates. *Front. Immunol.* 10, 256. doi: 10.3389/fimmu.2019.00256
- Xin, G., Wang, F., Zhao, L., Qin, Y., Huang, L., Yan, Q., et al. (2020). Integration of RNA-seq and RNAi provides a novel insight into the effect of *pvdE* gene to the pathogenic of *Pseudomonas plecoglossicida* and on the immune responses of orange-spotted grouper (*Epinephelus coioides*). *Aquaculture* 529, 735695. doi: 10.1016/j.aquaculture.2020.735695
- Xu, S., Peng, Z., Cui, B., Wang, T., Song, Y., Zhang, L., et al. (2014). FliS modulates FlgM activity by acting as a non-canonical chaperone to control late flagellar gene expression, motility and biofilm formation in *Yersinia pseudotuberculosis*. *Environ. Microbiol.* 16 (4), 1090–1104. doi: 10.1111/1462-2920.12222
- Yang, Q., Chu, Q., Zhao, X., and Xu, T. (2017). Characterization of IL-1 $\beta$  and two types of IL-1 receptors in miiuy croaker and evolution analysis of IL-1 family. *Fish Shellfish Immunol.* 63, 165–172. doi: 10.1016/j.fsi.2017.02.005
- Yokoseki, T., Iino, T., and Kutsukake, K. (1996). Negative regulation by FliD, FliS, and FliT of the export of the flagellum-specific anti-sigma factor, FlgM, in *Salmonella typhimurium*. *J. Bacteriol.* 178 (3), 899–901. doi: 10.1128/jb.178.3.899-901.1996
- Yokoseki, T., Kutsukake, K., Ohnishi, K., and Iino, T. (1995). Functional analysis of the flagellar genes in the *fliD* operon of *Salmonella typhimurium*. *Microbiology* 141, 1715–1722. doi: 10.1099/13500872-141-7-1715
- Zhang, M., Qin, Y., Huang, L., Yan, Q., Mao, L., Xu, X., et al. (2019). The role of *sodA* and *sodB* in *Aeromonas hydrophila* resisting oxidative damage to survive in fish macrophages and escape for further infection. *Fish Shellfish Immunol.* 88, 489–495. doi: 10.1016/j.fsi.2019.03.021
- Zhang, L., Song, M., Yang, N., Zhang, X., Abbas Raza, S., Jia, K., et al. (2020). Nucleoside diphosphate kinases (ndk) reveals a key role in adhesion and virulence of *Aeromonas veronii*. *Microb. Pathog.* 149, 104577. doi: 10.1016/j.micpath.2020.104577
- Zhang, L., Yao, Z., Tang, H., Song, Q., Song, H., Yao, J., et al. (2022). The lysine acetylation modification in the porin Aha1 of *Aeromonas hydrophila* regulates the uptake of multi-drug antibiotics. *Mol. Cell. Proteomics* 21 (9), 100248. doi: 10.1016/j.mcpro.2022.100248
- Zhao, L., Zhang, X., Qiu, Z., and Huang, Y. (2018). *De novo* assembly and characterization of the *Xenocatantops brachycerus* transcriptome. *Int. J. Mol. Sci.* 19 (2), 520. doi: 10.3390/ijms19020520
- Zuo, Y., Zhao, L., Xu, X., Zhang, J., Zhang, J., Yan, Q., et al. (2019). Mechanisms underlying the virulence regulation of new *Vibrio alginolyticus* ncRNA Vvrr1 with a comparative proteomic analysis. *Emerg. Microbes. Infect.* 18 (1), 1604–1618. doi: 10.1080/22221751.2019.1687261